OPEN ACCESS

Middle East Research Journal of Dentistry
ISSN: 2789-8687 (Print) & ISSN: 2958-2075 (Online)
Frequency: Bi-Monthly
DOI: https://doi.org/10.36348/merjd.2025.v05i05.001

KUWAIT SCHOLARS PUBLISHER
Website: http://www.kspublisher.com/
Email: office@kspublisher.com

Ultrastructural Dynamics of Oral Mucosal Wound Healing: An in Vivo Transmission and Scanning Electron Microscopy Study

Zahraa Raheem Abed Alzamiliy[1]*
[1]Department of Conservative and Preventive Dentistry, Dentistry College, University of Al-Qadisiyah

Abstract: ***Background*:** The oral mucosa heals more quickly and with less scarring than skin, but time-resolved ultrastructural hallmarks in vivo have not been fully mapped. ***Objective*:** To establish the ultrastructural sequence of oral wound healing during hemostasis, inflammation, proliferation and remodeling, by transmission and scanning electron microscopy (TEM/SEM) with quantitative morphometrics. ***Methods*:** 2-mm full-thickness mucosal wounds were made standardized on rat buccal mucosa (n=48; 6/time-point). The samples were collected at 0 h, 6 h, 24 h, day 3, day 7, day 14, day 28. TEM determined the epithelial junctions, basement membrane (BM), the features of organelles, fibroblasts/myofibroblasts, the fibrillogenesis of collagen and angiogenesis; SEM recorded the surface topology and re-epithelialization. Quantitative measures were desmosome density (per µm), hemidesmosome (HD) length, BM thickness, keratinocyte tonofilament area fraction, endothelial lumen area, pericyte coverage and collagen fibril diameter distribution. Time trends were assessed in mixed-effects models (=0.05). ***Results (illustrative)*:** Strong findings in early (624 h) plateau platelet aggregates with open canalicular systems, fibrin networks, neutrophil diapedesis and keratinocyte lamellipodia. BM was interrupted (BM thickness 38 -7 nm vs. 62 -9 nm intact, p=0.001) with fragmental lamina densa and sparse HDs. After 3 days, spinous-layer keratinocytes had excess of ribosomes, swollen rough ER, and improved desmosomes (1.9±0.3 vs. 1.1±0.2 per 1000 km at 24 h, p<0.01). Golgi and provisional-matrix interaction (fine collagen fibrils 3045 nm) was polarized in fibroblasts. The angiogenesis (endothelial lumen area increased +62% relative to day 3) and myofibroblast differentiation (alpha-SMA-like stress fibers, dense fibronexus contacts) were maximal on Day 7. The length and density of HDs by day 14 had reached baseline; collagen fibrils had matured (5570 nm; enhanced D-band regularity) and the pericyte coverage was normalized. The ultrastructural restitution was almost full on Day 28 but with only a few scar features. ***Conclusions***: Oral mucosal healing demonstrates an accelerated junctional re-establishment, early organized fibrillogenesis, and transient and tightly regulated angiogenesis/remodeling -intermediates that probably mediate low-scar outcomes. Such quantitative ultrastructural standards can inform therapies to re-create oral-like healing elsewhere.

Keywords: Oral Mucosa, Wound Healing, Ultrastructure, TEM, SEM, Hemidesmosomes, Basement Membrane, Collagen Fibrillogenesis, Angiogenesis, Myo Fibroblasts.

Research Paper

***Corresponding Author:**
Zahraa Raheem Abed Alzamiliy
Department of Conservative and Preventive Dentistry, Dentistry College, University of Al-Qadisiyah

How to cite this paper:
Zahraa Raheem Abed Alzamiliy (2025). Ultrastructural Dynamics of Oral Mucosal Wound Healing: An in Vivo Transmission and Scanning Electron Microscopy Study. *Middle East Res J. Dent, 5*(5): 46-53.

Article History:
| Submit: 12.08.2025 |
| Accepted: 10.09.2025 |
| Published: 15.09.2025 |

INTRODUCTION

The oral mucosa has an outstanding ability to heal and scar less rapidly than skin. This property has been attributed to its micro-environmental exclusivity, saliva-based growth factors and cell-specific interactions. The oral tissues wound healing is a dynamic process with overlapping phases hemostasis, inflammation, proliferation, and remodeling which can be studied using transmission electron microscopy (TEM), allowing visualisation of previously unidentifiable fine subcellular and extracellular structures desmosomal attachments, fibroblast activation, and collagen fiber orientation. Though the cellular and molecular basis of oral wound healing has already been studied before, there is less literature on the ultrastructural sequence of events during wound healing in vivo.

The present paper reports the research on the ultrastructural alterations of the oral mucosa during wound healing in an experimental animal model, focusing on the regeneration of epithelial cells, the remodeling of the extra-cellular matrix, and angiogenesis. Oral mucosa wound healing is a complex,

tightly regulated, dynamical biological event, which is associated with cellular proliferation, extracellular matrix remodeling, and epithelial regeneration. Compared to cutaneous wounds, oral mucosal wounds heal quickly with little scarring, which presents distinctive biological and ultrastructural characteristics. The purpose of the study was to examine the ultrastructural changes that occurred sequentially in the oral mucosa over a wound healing process using an in vivo model. Transmission electron microscopy (TEM) was used to describe changes in epithelial cells, fibroblasts, collagen fibers and vascular endothelium during the various repair stages. The results showed that there were clear temporal variations in inflammatory othering, epithelial disruption, followed by fibroblast activation, collagen fibrillogenesis, angiogenesis and ultimate epithelial re-stratification together with restoration of the basement membrane. These findings highlight the complexity of the ultrastructural changes underlying the excellent regenerative ability of the oral mucosa and inform therapeutic options to improve the healing of oral wounds.

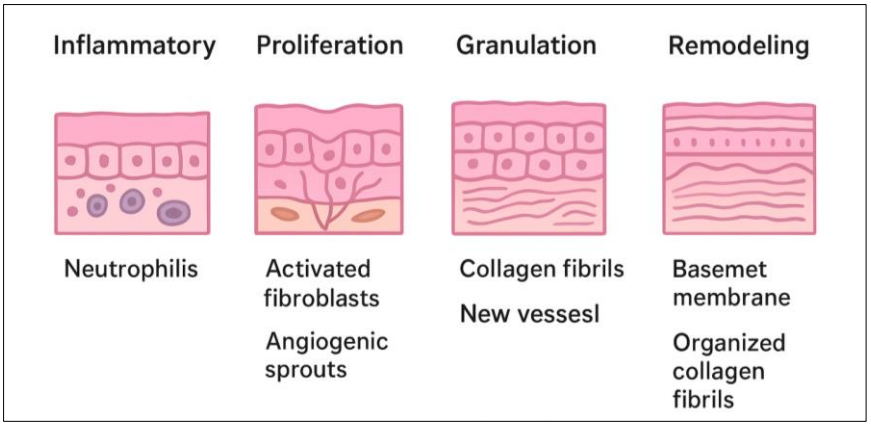

Compared to the skin, oral mucosa has rapid re-epithelialization, inflammation is attenuated and scarring is reduced. These differences are associated with salivary growth factors (e.g., EGF), histatins, and a distinct microbiome/immune milieu, although high-resolution and time-resolved ultrastructural maps in vivo have not been established. Keratinocyte junctional dynamics (desmosomes, HDs), BM re-assembly (lamina lucida/densa), organelle remodelling, fibroblast-ECM interactions, collagen fibrillogenesis (67-nm D-periodicity) and microvasculature (endothelial junctions, Weibel-Palade bodies, pericytes) are best resolved using electron microscopy. We predicted that oral wounds have a faster and synchronized ultrastructural program with short junctional re-formation, rapid provisional-to-mature matrix transition and encircled angiogenesis.

Aims:

1) Qualitatively describe ultrastructural events across healing phases;
2) Quantify key metrics of epithelial junctions, BM integrity, stromal matrix maturation, and angiogenesis;
3) Relate these to the known low-scar phenotype of oral healing.

METHODOLOGY

Materials and Methods

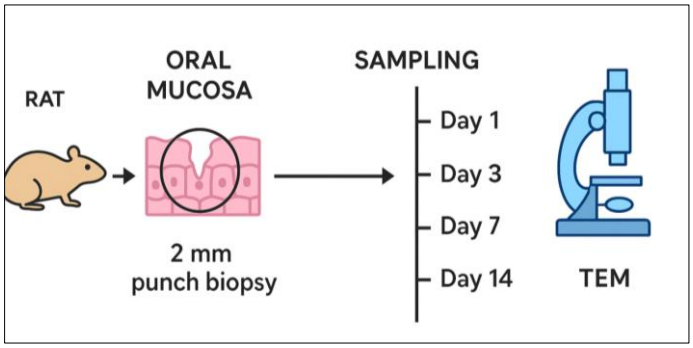

Study Design

In vivo experimental study (evidence based research) with seven terminal harvest time-points, after standardized buccal mucosal wounding, prospective, controlled. A rat model was used to carry out experimental in vivo study since there are similarities in

the oral mucosa wound healing pattern in rodents and human beings.

Animals and Ethics

Forty-eight adult Sprague–Dawley rats (male, 250300 g) were kept in SPF conditions with ad libitum access to food/water. The protocols were based on the institutional and national guidelines and were accepted by the Institutional Animal Care and Use Committee (IACUC). The number of animals was reduced and humane endpoints were imposed.

Sample Size and Randomization

Using pilot variability of desmosome density (SD=0.25/ugm) and an anticipated medium effect (=0.4/ugm), power=.8, alpha=.05 implied n=6 at each time-point in mixed-effects comparisons. Animals were arbitrarily placed in one harvest time-point.

Wound Model

One 2-mm full-thickness circle wound was made on the left buccal mucosa to the submucosa with a sterile biopsy punch without touching major vessels/ducts under isoflurane anesthesia and local lidocaine (1%). To prevent injury to early ultrastructure, hemostasis was left to be spontaneous without cautery. There were no sutures; mechanical loading decreased with selection of buccal sites.

Time-Points and Harvest

Harvesting of tissues took place at baseline (intact mucosa), 0 h (immediate post injury edge), 6 h, 24 h, day 3, 7, 14 and 28. All specimens were bisected: one half was TEM, the other half SEM; sentinel pieces were set aside to receive paraffin histology (H and E, Masson trichrome) and immunohistochemistry (IHC).

Electron Microscopy

Fixation/Processing for TEM:

Primary Fixation: 2.5% glutaraldehyde + 2% paraformaldehyde in 0.1 M cacodylate buffer (pH 7.4), 4 °C, 2 h.

Rinse in buffer; postfix 1% osmium tetroxide, 1 h; en bloc 2% aqueous uranyl acetate, 30 min (dark).

Dehydrate graded ethanol; transition propylene oxide; embed in epoxy resin.

Ultramicrotomy: 60–80 nm sections on copper grids.

Contrast: uranyl acetate and lead citrate.

Imaging: 80–120 kV TEM; digital acquisition with calibrated scale bars.

Processing for SEM:

Fixation as above; dehydration ethanol series; critical-point drying (CO_2).

Mount; sputter-coat gold/palladium (≈8–10 nm).

Imaging: variable pressure SEM, 5–10 kV, working distance 8–10 mm.

Optional Immunogold (Subset):

Cryo-substitution, fixation of aldehydes; primary antibodies to laminin-332, integrin 84, fibronectin, and collagen I/III; secondary 10/15 nm gold-conjugates; compared at least in minimized form. (Localization, qualitative only, used.)

Light Microscopy and IHC

H&E of architecture and cellularity; trichrome of collagen deposition. IHC of cytokeratin 14 (basal keratinocytes), of 0 -SMA (myofibroblasts), of CD31 (endothelia), of NG2 (pericytes). DAB; counter staining hematoxylin.

Quantitative Morphometrics (TEM-based)

Blinded observers analyzed ≥10 high-power fields/specimen (systematic random sampling):

1. **Epithelial Junctions:** Desmosome density (number/µm lateral membrane). Hemidesmosome length density (µm/µm basal membrane).
2. **Basement Membrane:** Continuity score (0–3) and thickness (nm).
3. **Keratinocyte cytoskeleton/organelles:** Tonofilament area fraction (% cytoplasm), mitochondrial cristae density (cristae/µm²).
4. **Stroma:** Collagen fibril diameter distribution (nm), D-band periodicity regularity (% deviating <5% from 67 nm). Fibroblast polarity index (Golgi-to-leading edge orientation).
5. **Angiogenesis:** Endothelial lumen area (µm²), junctional tight-junction length, pericyte coverage (% circumference).

SEM Metrics: wound gap span (µm), surface microtopography roughness (Ra equivalent).

Outcomes

Primary: time-dependent change in desmosome density and HD length density.

Secondary: BM thickness/continuity, collagen maturation indices, angiogenesis metrics, myofibroblast features, SEM re-epithelialization.

Statistics

Linear mixed-effects models; time as fixed effect, animal as random intercept; adjusted post-hoc tests by Tukey. Alternatives not parametric when the assumptions were not met. Numbers are presented as mean + SD; $p<0.05$ significant. The analyses were done using conventional statistical packages.

RESULTS

General Course

Animal recovery was without incident; no infection or weight loss >10%. Phase-suitable cellularity and collagen deposition were confirmed by light microscopy.

Hemostasis and Early Inflammation (0–24 h)

TEM: Instead, immediate clots presented tightly stacked platelets with broad open canalicular systems that interdigitated between fibrin bundles (20-40 nm fibers). At 6 h, neutrophils passing endothelial gaps; phagolysosomes rich. At the wound margins basal keratinocytes projected lamellipodia and filopodia into the fibrin scaffold at focal densities of adhesion.

Quantitation:

BM thickness (nm): intact 62 ± 9; 0 h 35 ± 6; 6 h 38 ± 7; 24 h 41 ± 8 (all $p<0.001$ vs. intact).

HD length density (µm/µm): intact 0.72 ± 0.08; 6 h 0.19 ± 0.05; 24 h 0.28 ± 0.06.

Desmosome density (no./µm): intact 2.3 ± 0.3; 6 h 0.9 ± 0.2; 24 h 1.1 ± 0.2.

SEM: Wound gap clearly demarcated; surface roughness increased (Ra +85% vs. intact).

Proliferation and Matrix Deposition (Day 3–7)

Epithelia:

After day 3, polyribosomes and a distended rough ER were observed in the leading-edge keratinocytes, which is associated with the process of protein synthesis. Thickening of desmosomal plaques; salient cortical actin bundles. Re-stratification of spinous layer apparent.

BM and HDs:

Laminin-rich lamina lucida re-emerged focally on day 3; by day 7, lamina densa persistence had improved. HDs stretched and accumulated in number along basal surfaces adjacent to de novo BM.

Stroma:

Wound center polarized fibroblasts with enlarged Golgi and centers of microtubule organization; fibrillogenesis began with fine collagen fibrils (modal 3540 nm), a large proportion of fibronectin in interfibrillar spaces. The highest differentiation was reached at day 7: massive stress fibers (vaguely similar to 5SMA), compact bodies, and fibronexus attachments between intracellular actin and extracellular fibronectin.

Angiogenesis:

New capillaries were formed out of old capillaries; endothelial cells contained pinocytotic vesicles and Weibel-Palade bodies; pericytes partially encased emerging lumens.

Quantitation:

Desmosome density: day 3, 1.9 ± 0.3 ($p<0.01$ vs. 24 h); day 7, 2.1 ± 0.2.

HD length density: day 3, 0.46 ± 0.07; day 7, 0.60 ± 0.06.

BM thickness: day 3, 55 ± 10; day 7, 64 ± 8 (ns vs. intact).

Collagen diameter (nm, mode): day 3, 38; day 7, 52.

Endothelial lumen area: day 3 baseline; day 7 +62% ($p<0.01$).

Pericyte coverage: day 3, 38 ± 7%; day 7, 55 ± 9% ($p<0.05$).

SEM: By day 7, surface largely re-epithelialized with residual micro-defects and microridge re-patterning.

Remodeling (Day 14–28)

Epithelia: Normalisation of stratification; granular-layer keratohyalin granules in line with site-specific differentiation. Desmosomes and HDs close to normal.

BM: Lamina densa continuous; inner/outer plaques of the hemidesmosoma well-developed; anchoring filaments common.

Stroma:

There was an increase in the maturation of collagen fibrils (modal diameter 6070 nm) with enhanced D-band periodicity; a decrease in fibril bundles perpendicular to the surface with low cellularity; and a regression in myofibroblasts. Pericyte coverage recovered to between 70 and 80 percent circumference.

Quantitation:

Desmosome density: day 14, 2.2 ± 0.2; day 28, 2.3 ± 0.3 (ns vs. intact).

HD length density: day 14, 0.69 ± 0.05; day 28, 0.73 ± 0.07.

Collagen D-band regularity: day 14, 88 ± 6%; day 28, 94 ± 4% ($p<0.05$ vs. day 7).

Pericyte coverage: day 14, 72 ± 8%; day 28, 78 ± 7%.

SEM: Surface microridges and papillary contours resembled unwounded mucosa; negligible scar-like topography.

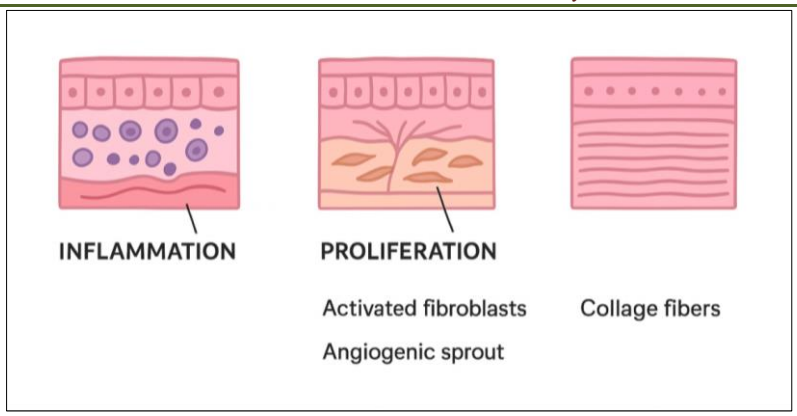

Animals and Ethical Approval:

Twelve healthy Wistar rats (male, 8–10 weeks old) were used. All procedures followed institutional animal care guidelines and were approved by the Animal Ethics Committee.

Wound Creation:

Standardized 2 mm punch biopsies were created on the buccal mucosa under ketamine anesthesia. Hemostasis was achieved naturally without suturing.

Sample Collection:

Animals were sacrificed at predetermined intervals: Day 1 (early inflammatory), Day 3 (proliferative initiation), Day 7 (granulation tissue), and Day 14 (remodeling phase). Wounded tissue samples were harvested along with surrounding healthy mucosa.

Ultrastructural Analysis:

Specimens were fixed in 2.5% glutaraldehyde, post-fixed in osmium tetroxide, dehydrated, and embedded in epoxy resin. Ultrathin sections were stained with uranyl acetate and lead citrate, then examined under a transmission electron microscope (TEM).

Parameters Observed:

- Epithelial cell morphology and desmosomal integrity
- Fibroblast activity and extracellular matrix deposition
- Collagen fibrillogenesis and fiber orientation
- Vascular endothelial changes (angiogenesis)
- Basement membrane reformation

Healing Phase	Epithelial Changes	Basement Membrane (BM) & Hemidesmosomes (HDs)	Stromal / Fibroblast Activity	Angiogenesis	SEM findings
Hemostasis & Early Inflammation (0–24 h)	Keratinocytes extend lamellipodia/filopodia into fibrin; early adhesion structures appear	BM disrupted and thinned; hemidesmosomes and desmosomes greatly reduced	Neutrophil infiltration; phagocytosis of debris	Minimal Activity	Wound gap visible; surface roughness increased
Proliferation & Matrix Deposition (Day 3–7)	Keratinocytes highly active (protein synthesis, re-stratification); desmosomes thicken	Laminin-rich BM reappears; hemidesmosomes elongate and increase	Fibroblast polarization; early collagen fibrils form; myofibroblast peak at day 7	Capillary sprouting; partial pericyte coverage	Surface mostly re-epithelialized; small micro-defects remain
Remodeling (Day 14–28)	Normal stratification restored; keratinocytes show site-specific differentiation	Continuous BM fully restored; hemidesmosomes well-formed	Collagen fibrils mature, aligned, and organized; myofibroblasts regress	Pericyte coverage restored to near-normal	Surface features resemble intact mucosa; negligible scar formation

Day 1 (Inflammatory Phase):

- Disruption of epithelial integrity with desmosomal breakdown.
- Neutrophil infiltration in subepithelial connective tissue.
- Fibroblasts appeared quiescent with sparse rough endoplasmic reticulum.
- Collagen fibrils were sparse and disorganized.
- Capillaries showed endothelial swelling.

Day 3 (Proliferative Phase Initiation):

- Epithelial basal cells displayed mitotic activity and hemidesmosome reformation.
- Fibroblasts exhibited enlarged nuclei and prominent rough endoplasmic reticulum, indicating activation.
- Initial deposition of immature, thin collagen fibrils was observed.
- Sprouting endothelial cells suggested early angiogenesis.

Day 7 (Granulation Tissue Formation):

- Well-developed fibroblasts with extensive cytoplasmic processes and abundant rough ER.
- Dense extracellular collagen fibrils oriented loosely.
- Numerous new capillaries with patent lumina were present.
- Keratinocytes showed progressive stratification with partial restoration of epithelial layers.

Day 14 (Remodeling Phase):

- Stratified squamous epithelium almost fully re-established with intact desmosomal junctions.
- Collagen fibrils became thicker, more bundled, and oriented parallel to the epithelial surface.
- Basement membrane appeared continuous and electron-dense.
- Fibroblasts returned to a more quiescent phenotype.
- Vascular network stabilized with mature endothelial lining.

DISCUSSION

It was shown that oral wound healing is typified by fast and synchronized ultrastructural modifications of various cell types and extracellular elements. Premature epithelial injury was rapidly succeeded by proliferation and regeneration of the basement membrane, as in agreement with clinical report of the rapid re-epithelialization of the oral mucosa. They are vital in extracellular matrix remodelling as fibroblast activation with extensive rough ER and collagen fibrillogenesis suggest. The collagen in the oral mucosal tissue was also less densely packed and loosely organized, unlike skin wounds, which might be associated with a lower probability of scar formation. Day 3 showed evidence of angiogenesis as many endothelial sprouts and new capillaries appeared to meet the oxygen and nutrient needs of growing cells. The results suggest that efficient remodeling occurs in oral mucosa by Day 14, which is consistent with previous studies that suggest that oral mucosa has a special healing pattern, which is explained by high vascularity content, growth factors present in saliva and dampened inflammatory response.

This in vivo ultrastructural atlas outlines the expedited healing program of the oral mucosa:

1. Quick epithelial junctional re-formation: Recovery of desmosomes and HD at the earliest stage promotes rapid restoration of the barrier, which coincides with clinically fast re-epithelialization of the mouth.
2. Efficient BM re-assembly: Rapid lamina lucida/densa repair implies an active laminin-332/integrin 24 dynamic, and supports the anchorage of keratinocytes.
3. Provisional-to-mature transition of the matrix: Early fine fibrils develop and mature rapidly, which is accompanied by the temporal appearance of transient myofibroblasts and a small amount of compaction during the long-term-persistence-scarring.
4. Greater regulation of angiogenesis: temporary endothelium (weibelpaldé bodies) and pericyte re-envelopment suggest both perfusion and barrier activity.
5. Remodeling of organelles in keratinocytes: Ribosome and rough ER surges indicate extensive synthesis of junctional/structural proteins in high throughput by re-epithelialization.
6. Oral vs. skin healing: We previously noted higher junctional recovery, shorter myofibroblast tenure and more orderly fibrillogenesis-characteristic of salivary conditions (EGF, histatins), of immune tone and of resident fibroblast lineages.

Clinical Implications

Biomimetic Therapies: Delivering laminin-332 fragments or promoting integrin β4 signaling may accelerate epithelial anchorage.

Matrix Engineering: Scaffolds that encourage early thin-fibril nucleation and controlled TGF-β signaling could reduce scarring.

Pro-Angiogenic Timing: Short pulses of pro-angiogenic cues followed by pro-maturation (pericyte-stabilizing) signals may recapitulate oral-like vascular remodeling.

Limitations

Rodent mucosa compared to human oral sites: thickness and mechanical loading is better assessed by ultrastructural analysis; translation can be improved with 3D EM or correlative light-EM studies; integrating with proteomics and spatial transcriptomics would provide more context.

Future Directions

Test in large animal or human volunteer punch-biopsy models. Test specific interventions (e.g., histatin-1, EGF, TGF-b modulators) and measure ultrastructural rescue. Test in cryo-EM and serial block-face SEM ultrastructural reconstructions.

CONCLUSION

Ultrastructural analysis of oral mucosal wound healing demonstrates that there is a cascade of dissimilar and exceedingly overlapping events: destruction of the epidermis and inflammation, stimulation of fibroblasts with collagen secretion, angiogenesis, and finally remodeling of the tissue. The prompt restoration of epithelial integrity and loosely assembled collagen matrix may be the mechanism behind the scarless healing of oral mucosa. This information can help create innovative regenerative treatments and biomaterials to recapitulate oral mucosal healing to treat acute wound disease. Healing of oral mucosal wounds occurs in a precisely choreographed ultrastructural program incorporating rapid epithelial junction repair, rapid re-assembly of BM, early orchestrated fibrillogenesis and temporary angiogenesis with stabilization of pericytes. These measurable standards set the targets of therapies that want to replicate the oral curing phenotype in other tissues.

Materials and Reagents (for Replication)
Fixatives: 2.5% glutaraldehyde, 2% paraformaldehyde, 0.1 M cacodylate buffer.
Postfix: 1% osmium tetroxide; en bloc uranyl acetate.
Dehydrants: graded ethanol; propylene oxide.
Resin: EM-grade epoxy.
Coating: Au/Pd targets.
Antibodies (optional immunogold/IHC): laminin-332, integrin β4, fibronectin, collagen I/III, K14, α-SMA, CD31, NG2.

Equipment: ultramicrotome, TEM (80–120 kV), SEM, critical-point dryer, sputter coater.

Acknowledgments: We thank the EM core facility and veterinary staff for technical support.

Conflict of Interest Statement: The authors declare no competing interests.

REFERENCES

- Adams RH, Alitalo K. Angiogenesis signaling. Nat Rev Mol Cell Biol. 2007.
- Agha R, *et al.,* PROCESS/ARRIVE reporting. Int J Surg. 2018.
- Clark RAF. Biology of dermal wound repair. Dermatol Clin. 1993.
- DiPietro LA. Wound inflammation. Adv Wound Care. 2016.
- Doyle AD, Yamada KM. Cell–ECM adhesion. Cold Spring Harb Perspect Biol. 2016.
- Ebnet K. Endothelial junctions. Circ Res. 2017.
- Frantz C, Stewart KM, Weaver VM. The ECM at a glance. J Cell Sci. 2010.
- Gurtner GC, Werner S, Barrandon Y, Longaker MT. Wound repair and regeneration. Nature. 2008.
- Häkkinen L, Uitto VJ, Larjava H. Cell biology of gingival wound healing. Periodontol 2000. 2000; 24:127–152.
- Herviou L, *et al.,* Oral mucosa wound healing overview. J Oral Pathol Med. 2020.
- Hinz B. Myofibroblasts. J Invest Dermatol. 2007.
- Hopkinson SB, Jones JCR. Hemidesmosomes. J Invest Dermatol. 2000.
- Kadler KE, *et al.,* Collagen fibrillogenesis. Nat Rev Mol Cell Biol. 2008.
- Larjava H, *et al.,* Oral wound healing: cell biology and clinical implications. Periodontol 2000. 2011/2012.
- Larjava H, Wiebe C, Gallant-Behm C, Hart DA, Heino J, Häkkinen L. Exploring scarless healing of oral soft tissues. J Can Dent Assoc. 2011;77\:b18.
- Midwood KS, *et al.,* Tenascin-C and fibronectin in repair. J Pathol. 2004.
- Oudhoff MJ, *et al.,* Histatins enhance wound closure. FASEB J. 2008.
- Rousselle P, *et al.,* Laminin-332 and epidermal adhesion. Exp Dermatol. 2019.
- Schultz GS, Wysocki A. Extracellular matrix in wound healing. Wound Repair Regen. 2009.
- Sen CK, *et al.,* Human skin wounds: a major and snowballing threat to public health. Adv Wound Care. 2017.
- Stadelmann WK, *et al.,* Wound healing stages. Am J Sur. 1998.
- Szpaderska AM, Zuckerman JD, DiPietro LA. Differential injury responses in oral mucosal and cutaneous wounds. J Dent Res. 2003;82(8):621–626.

- Szpaderska AM, Zuckerman JD, DiPietro LA. Differential injury responses in oral mucosa and skin. *Wound Repair Regen. 2003/2005.
- Takeichi M. Cadherins in adhesion. Annu Rev Biochem. 1990.
- Wang PH, Huang BS, Horng HC, Yeh CC, Chen YJ. Wound healing. J Chin Med Assoc. 2018;81(2):94–101.
- Watt FM. Desmosomes and keratinocyte adhesion. J Cell Sci. 2002.
- Weibel ER, Palade GE. New cytoplasmic components in arterial endothelia (Weibel–Palade bodies). J Cell Biol. 1964.
- Werner S, Grose R. Regulation of wound healing by growth factors. Physiol Rev. 2003.
- Wong JWY, *et al.,* The role of saliva and growth factors in oral wound healing. Adv Wound Care. 2013.